CONGENITAL HEART DISEASE

# Quantifying regional right ventricular function in tetralogy of Fallot

JONDAVID MENTEER, M.D.,[1,*] PAUL M. WEINBERG, M.D.,[2] and MARK A. FOGEL, M.D.[2]

[1]*Division of Cardiology, Children's Hospital Los Angeles, Los Angeles, California, USA*
[2]*The Cardiac Center, Children's Hospital of Philadelphia, Philadelphia, Pennsylvania, USA*

Right ventricular (RV) function is notoriously difficult to quantify. Patients with tetralogy of Fallot (TOF) have decreased systolic performance. We measure regional RV performance using MRI with 1-dimensional myocardial tissue tagging. By tagging cine-MRI in two views, we measured regional shortening in 12 regions throughout the RV. We image 32 pediatric patients: 21 normal patients and 11 patients with repaired TOF. We establish a normal range for each RV region. TOF patients have decreased shortening on a region-by-region basis. We conclude that regional RV performance can be measured using this technique, and that decreased performance can be demonstrated in TOF patients.

*Key Words:* Magnetic resonance imaging; Tetralogy of Fallot; Myocardial contraction; Systole; Mechanics

## 1. Introduction

Right ventricular (RV) function has been notoriously difficult to quantify, and regional RV performance is even more difficult to measure objectively. Regional function of the RV is important to assess in pathologic states of congenital heart disease such as anomalous coronary artery origins, postoperative congenital heart disease (e.g. tetralogy of Fallot [TOF]), systemic right ventricles (e.g. transposition of the great arteries after Mustard operation or hypoplastic left heart syndrome after palliative surgery), or transplant vasculopathy. Current imaging tools that provide methods for quantitative assessment of global RV function include angiography, radionuclide ventriculography, magnetic resonance imaging (MRI), and echocardiography (1–6). There is currently no standardized tool for quantification of the regional function of the RV, although angiography (7), MRI (8–11) and tissue Doppler echocardiography (12–14) have been used in past studies.

MRI with tissue tagging has been used to evaluate many aspects of LV function, including regional systolic function (15–18) wall thickening, and systolic (14, 19) and diastolic strain (20). Grid (2-D) tagging of the myocardium is more commonly utilized for LV, but because the RV wall is normally much thinner than the LV, grid tagging of the RV results in many incomplete tags which are not useful for analysis. This limitation in 2-D tagging led us to utilize 1-D tags for this study. Although imaging of the RV with 1-dimensional (1-D) tagging in 4-chamber view has been demonstrated, no analysis of RV function has been done on this basis (21). Similar techniques have been used for qualitative assessment of regional wall motion within the heart, and such techniques have imaged the RV, but analysis of regional function has focused only on the left ventricle rather than the RV in these studies (16, 18).

Multiple studies have shown that global RV function is reduced in patients after repair of TOF (22, 23). One contributing factor to this dysfunction is the volume load imposed by pulmonary insufficiency (PI) (6, 24–27). In fact, when the volume load is removed by placing a competent pulmonary valve in the RV outflow tract, RV function improves (22, 24). Regional RV performance in these patients has not been described and would be important to understand.

The purpose of this study was to evaluate regional RV systolic function of the volume-loaded RV, using postoperative TOF heart with pulmonary insufficiency as a model of a volume load, and to compare this to a group of normal RVs.

## 2. Materials and methods

Permission to conduct this study was granted by the Institutional Review Board at The Children's Hospital of Philadelphia.

1097-6647 © 2005 Taylor & Francis Inc.

## 2.1.  *Patients*

Twenty-one subjects, ages 15 days to 25 years (median 9.2 years), underwent cardiac MRI for evaluation of clinical signs and symptoms and were found to have normal cardiac structure and function. In addition, 11 patients with TOF, ages 63 days to 21 years (median 11.5 years), with varying degrees of pulmonary insufficiency, were also evaluated by cardiac MRI. All patients underwent cardiac MRI for clinically indicated purposes between November of 2001 and March of 2003.

## 2.2.  *MRI*

Studies were performed on Siemens' 1.5T Vision and Sonata systems (Siemens Medical Systems, Malvern, PA, USA). All patients were in normal sinus rhythm. Patients under 8 years of age were sedated for the procedure using IV midazolam, and received standard monitoring including electrocardiography (ECG), pulse oximetry, and video surveillance.

## 2.3.  *Protocol*

After localizing sequences were performed, a set of $T_1$ spin echo or static True-Fast Imaging with Steady state Precision (true-FISP) axial images spanning the entire chest were acquired for assessment of anatomy. For $T_1$ images, the effective repetition time (TR) was the R-R interval (generally 350–1000 ms), the echo time (TE) was 15 ms, the number of excitations (NEX) was 2, the image matrix size was $128 \times 256$ pixels interpolated to $256 \times 256$ pixels, the field of view (FOV) ranged from 180–400 mm, and the slice thickness ranged from 3–8 mm. True-FISP imaging used a modified single-shot technique, where 29–51 lines of k-space were acquired in each heart beat in late diastole. Our Sonata machine segmented images to 5 lines of k-space per heartbeat. The TR was defined as the amount of time to acquire these lines of k-space, and typically ranged from 150–230 ms. Trigger delay typically ranged from 300–700 ms. TE was 1.3–1.8 ms, NEX was 3, matrix ranged from $100 \times 128$ to $256 \times 256$. Other imaging parameters were the same as $T_1$ spin echo imaging.

Further imaging was acquired as dictated by clinical scenario. For TOF patients, this included phase-contrast velocity mapping in the main and branch pulmonary arteries. From these velocity maps, the forward and reverse flow in the main pulmonary artery were calculated in order to generate a pulmonary regurgitant fraction (28).

After the axial images were obtained, multiplanar reconstruction was used to select oblique planes and slice positions to determine a 4-chamber (4ch) view and RV long axis (RVLA) view. The 4ch view was obtained by defining the atrioventricular valve (AVV) plane and the apex and then creating a plane which bisects the middle of the AVV plane and the apex. In addition, the RVLA was established by defining a superoinferior plane perpendicular to the 4ch view, which bisects the tricuspid valve and the apex of the RV.

Two cine sequences (one in the 4ch view, the second in the RVLA view) were performed using 1-D tagging. 1-D tags are a set of parallel stripes generated by a saturation pulse laid down at the beginning of the cardiac cycle prior to imaging (Fig. 1). This pre-pulse destroys the proton alignment in the stripes, resulting in a signal void (dark line) on the image. The prepulse was applied at end-diastole in an orientation perpendicular to the ventricular long axis, parallel to the AVVs, and therefore perpendicular to the apparent major axis of in-plane travel of the myocardium. Fourteen to 28 phases of the cardiac cycle immediately following the tagging prepulse were acquired, depending on heart rate. Seven to 13 of these frames were systolic. This temporal resolution allowed adequate estimation of end systole, while minimizing the signal degradation associated with higher sampling rates. In order to obtain a relatively consistent number of frames per cine, despite a wide variation in heart rates between patients, the frame rate (number of frames per second) was indexed to heart rate.

The following parameters were used for cine sequences: TR= 350–1000 ms, TE=7 ms, NEX=2, slice thickness 5–8 mm, number of slices 3, slice spacing 3–5 mm, FOV 200–250 mm, tag thickness 1.5–2 mm, distance between tags 6–10 mm, matrix $128 \times 256$ interpolated to $256 \times 256$ pixels. During systole, in-plane myocardial motion brings the stripes closer together, and this regional shortening was quantified.

## 2.4.  *Image and data analysis*

Images were analyzed using the VIDA software package (Division of Physiologic Imaging, Department of Radiology, University of Iowa College of Medicine) on a Sun SPARC 10 workstation (Santa Clara, CA, USA) (30). On each tagged image sequence (4ch and RVLA), 6 regions were standardized for analysis, for a total of 12 regions. On the 4ch view, 3 regions along the RV freewall (AVV, mid, and apex), and 3 regions along the septum (AVV, mid, and apex) were defined; on the RVLA view, 3 regions along the superior wall (RVOT, mid, apex) as well as 3 regions along the inferior wall (AVV, mid, apex) were defined.

Within each region, a line was drawn through a pair of myocardial tags, parallel to the direction of myocardial motion, and an "intensity map"—a graph of the signal intensity at each pixel along the defined line—was generated along this line which allowed precise identification of the center, or darkest portion (lowest signal intensity), of each stripe (Fig. 1). The distance between the stripes in each of the 12 regions through all systolic phases were measured. End systole was defined as the time when maximal shortening had occurred for the region being measured.

When the distance between the stripes in each region at end diastole (ED) and end systole (ES) were obtained, a regional shortening fraction (RSF) for each region was calculated using:

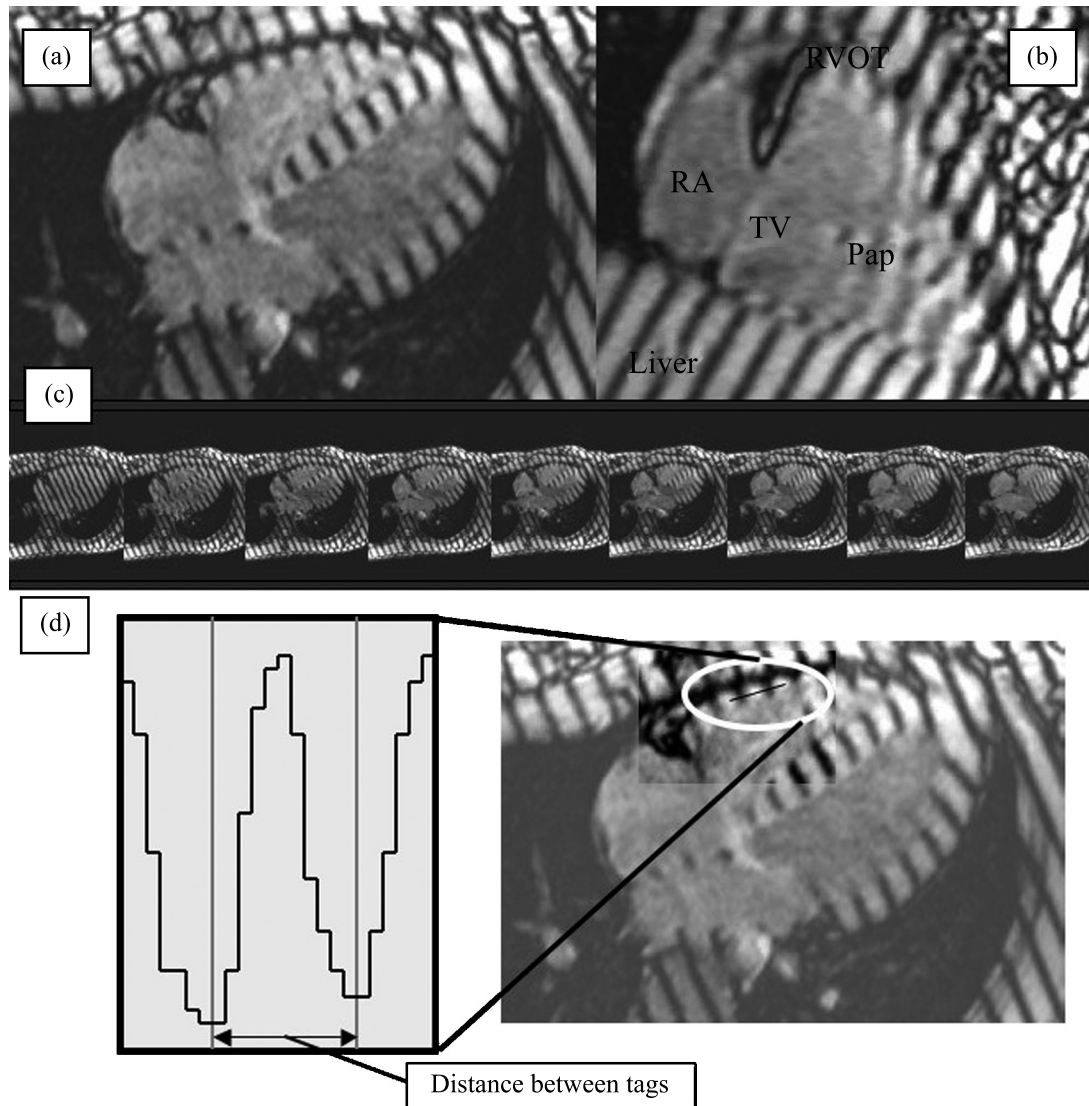$$RSF = (ED - ES)/ED \times 100\% \qquad (1)$$

**Figure 1.** 1-D myocardial tagging and intensity mapping. (a) 4 chamber view, (b) RV long axis view. Right atrium (RA), tricuspid valve (TV), papillary muscle of the RV (pap), right ventricular outflow tract (RVOT). The RV wall is thin but discernable in this image along the diaphragm, and from the apex to the RVOT. (c) Systolic frames from one tagged cine-MRI sequence, demonstrating tags becoming closer during systole. (d) Intensity Mapping. A line is drawn between stripes, designating the measurement of interest. The VIDA program draws a graph of the grey-scale intensity of every pixel along the line, allowing precise identification of the centers of each dark stripe. The program uses embedded data to calculate the distance between two points on the line. The change in the distances between stripes during systole is used to calculate the RSF.

ED distances were defined on the first (ECG-gated) frame of the cine. The ES frame of the cine was defined as the frame in which the stripes had reached their nearest distance. This was determined independently for each region. Since some regions may have reached full contraction earlier or later in the cardiac cycle, especially in TOF patients with right bundle branch block, our RSF measurements represent the maximum regional shortening for each region. In rare cases, the image quality in a few regions did not allow for accurate calculation of end-systolic distances, and these regions were dropped from the analysis. In all patients, but in TOF patients with dilated RVs in particular, the ventricular wall may be curved

significantly. This curvature did not alter our ability to interpret stripe position. When a stripe was positioned at a slightly oblique angle through a particular segment of the RV, the position of the stripe at the center of the RV wall was used as the reference point.

In addition to RSF, an average of all RSFs for each patient was calculated as a "composite RSF." This allowed a comparison of a single index of all of the RSFs with the degree of pulmonary insufficiency in the TOF patients. Although the traditional ejection fraction would have also served as a measure of global RV contraction, we sought a measure to index the average maximal regional shortening of

the regions. In patients with right bundle branch block, some regions had entered diastole before the end of systole for other regions; thus, some work done by late-contracting regions may not be translated into increasing ejection fraction.

In order to index the performance of each region of the RV in another way independent of RSF, we determined the time to reach 70% of total systolic contraction (t70). First, we calculated the distance between stripes when 70% of systolic contraction had occurred (d70) using the formula:

$$d70 = ED - [(ED - ES) * 0.70] \qquad (2)$$

Second, the earliest frame in the cine was found where the distance between stripes was less than or equal to d70. This frame number was compared to the total number of systolic frames in the cine (as defined above), and the t70 was expressed as a percentage of the time in systole. For example, if ED was 10 mm, and ES was 7 mm (an RSF of 30%), then d70 was 7.9 mm. If the first frame in the cine where stripes in this region were less than or equal to 7.9 mm apart was the 10th of 16 frames, then t70 was 63%. Regions with low t70 contract more quickly than regions with lower t70, regardless of the RSF in that region. Because of the very heterogeneous depolarization of the RV in postoperative TOF patients, nearly all of whom have right bundle-branch block, this analysis was conducted only on normal patients.

## 2.5. Statistics

The mean RSF and standard deviation for each of the 12 regions was calculated for the normals and TOF patients. The regional shortening was compared within each patient population using one-way repeated measures ANOVA analysis, and subsequent paired analysis when applicable. Regional shortening comparison between patient populations was performed using two-way repeated measures ANOVA, which allows for differences between regions. Subsequent paired analysis was performed when applicable. In order to correlate regional shortening with volume loading conditions, pulmonary insufficiency versus regional shortening comparisons were made using Pearson product correlation and linear regression.

**Table 1.** Patient populations

|  | Normals | TOF | P |
|---|---|---|---|
| N= | 21 | 11 | |
| Age | 15d to 22.5 yrs (Median 9.2 yrs) | 63d to 21.4 yrs (Median 11.5 yrs) | NS |
| Sex—M:F | 13:8 | 5:6 | |
| Pulmonary Regurgitant Fraction | N/A | 4–93% (Median 35%) 9 of 11 > 29% | |

## 3. Results

Patient characteristics for normal and TOF groups are summarized in Table 1. For the normal group, the median age was 9.2 years (range, 15 days to 22.5 years). For the TOF group, the median age was 11.5 years (range 63 days to 21.4 years, p = NS). No patients had greater than mild valvar or branch pulmonary stenosis as subjectively assessed.

In the TOF group, surgical histories were available for 10 of 11 patients. One patient had not received surgical treatment and for another patient no surgical data was available. The mean time since initial surgery was 4.9 years (range 2 weeks to 13 years). Two of 11 patients required reoperation after their initial surgery, and both of these patients were > 10 years from their most recent surgery at the time of MRI study.

Our technique was successful in producing interpretable data. Tissue tags always degrade during the course of the cardiac cycle, but, in general, stripe degradation was not problematic during systole. The contrast between light and dark signal often became poor in the (unused) diastolic images. Twelve point eight percent of data from TOF patients and 10.8% of data from normal patients could not be analyzed because of poor quality images. We found that the stripes and images were sharpest using our Sonata machine.

### 3.1. Normal regional RV mechanics

The average regional shortening fractions and standard deviations for each of the 12 regions are included in Fig. 2. One-way repeated measures ANOVA revealed significant differences between regional shortening fractions ($p = 1.01 \times 10^{-17}$) and paired analysis revealed significant different between each freewall region (AVV, Mid, and Apex) and each septal regions (AVV, Mid, and Apex) (p for all < .05). Along the inferior wall, the apex had greater shortening than the AVV (p < .05), and also had greater shortening than all septal regions (p < .05). The inferior AVV had significantly less shortening than any of the freewall regions (p < .05). There were differences between the RSF at the AVV level, with greater shortening demonstrated by the freewall portion than along the inferior AVV (p < .05). At the apex, the freewall performed better than the superior wall (p < .05), with the inferior wall displaying intermediate shortening. (p = NS).

Upon frame-by-frame analysis of regional contraction of the RV, one-way repeated measures ANOVA did not reveal significant differences in the time to 70% of total shortening (t70). A typical patient's regional contraction is shown in Fig. 3. Within each patient there was variability in the t70 between regions. The overall average t70 was 65% of systole ± 16% (95% confidence limits, 33% to 97%) (Fig. 4). The wide confidence intervals were *not* due to small numbers of outlying patients. Rather, each patient had wide ranges of t70's between regions. For example, one patient had rapid contraction of the inferior wall, with t70 of 25% in the mid and apical inferior wall, while the septal AVV had slow
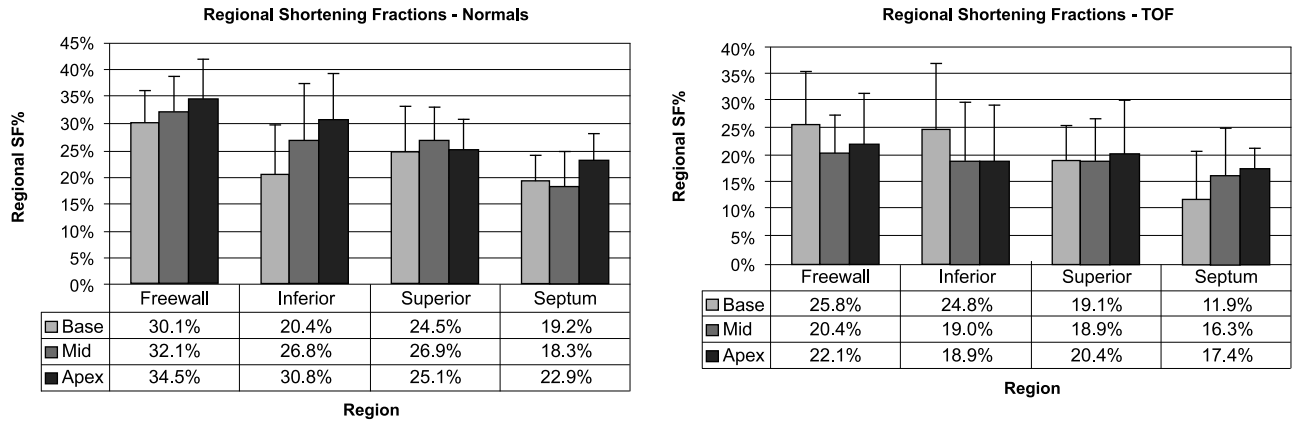
**Figure 2.** Average Regional Shortening Fractions (RSF) in normal patients and in TOF.

contraction, not achieving t70 until 87% of systole was completed. In another patient, the superior apex contracted rapidly, with a t70 of 42%, while the adjoining region at the superior apex had a t70 of 86%. While our limited temporal resolution may have affected measurement of t70, these region-to-region differences exceeded the $10-20\%$ variability we expected based on our sampling rate. Because of the significant multi-factorial variability of the t70 within the normal patients and because of the heterogeneous depolarization of the ventricle in the setting of a right bundle-branch block, this parameter was not measured for the TOF patients.

### 3.2. *Regional RV mechanics in tetralogy of Fallot*

The average regional shortening fractions and standard deviations are summarized in Fig. 2. One-way repeated measures ANOVA revealed significant differences between regional shortening fractions in various regions (p=.003). Subsequent paired analysis revealed significant differences

between a number of freewall and septal regions (p for all < .05). The inferior AVV displayed significantly greater shortening than the AVV septum. Frame-by-frame analysis of the TOF patients was not performed because of confounding factors regarding RV conduction delays in these patients.

### 3.3. *Effect of pulmonary insufficiency and operative status*

The pulmonary regurgitant fraction (PRF) was measured in 10 of 11 TOF patients. One patient did not have this measurement performed because a stent in the patient's main pulmonary artery prevented adequate quality velocity mapping. Of the ten patients measured, the average PRF was 37% (range 4 to 93%). Pulmonary insufficiency correlated inversely with regional shortening in the mid and apical septum (Fig. 5) using the Spearman method (r = $-$ 0.72 and $-$ 0.75, and p = .02 and .01, respectively). Figure 5 also illustrates PRF vs. the average (composite) regional shortening fraction for each patient. Linear regression analysis
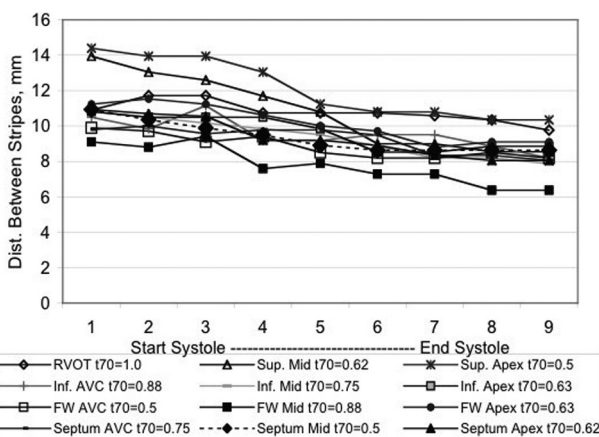


**Figure 3.** Frame by frame analysis of regional RV contraction in one normal patient. Note that some regions begin to contract immediately after the beginning of systole, while other regions do not shorten until the 3rd or 4th frame of the cine. There was no consistent order of regional contraction from patient to patient.
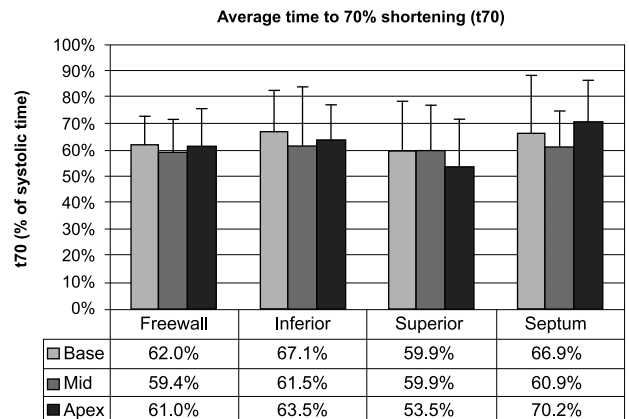


**Figure 4.** Average time to 70% shortening for normal RV regions. Error bars represent one standard deviation. There were no significant differences between regions.

reveals a relationship between PRF and composite regional shortening fraction, with lower RSFs seen in patients with higher PRFs (Pearson method, R = 0.60); but this was not strong enough to achieve significance in correlation testing (Pearson method, p = .09). There was no relationship between patient age and composite RSF.

Surgical history was known for 10 of the 11 patients with TOF. Three patients were over 10 years post-op from both initial and last operation, no patients were 5–10 years post-op, 5 patients were < 5 years post-op, and one patient was known unoperated. Average composite shortening fractions were calculated for these four groups of patients. The average was 20% for patients > 10 years post-op, 18% for patients 0–5 years post-op, and the unoperated patient had an composite SF of 22%. There was no statistically significant difference between these groups. The regional shortening of the unoperated patient was more similar to other TOF patients than to normal patients on a region by region basis.

### 3.4. *Comparing normals and TOF patients*

The normal and TOF patient data are compared graphically in Fig. 6. Two-way repeated measures ANOVA revealed a

**Figure 6.** Comparison of regional shortening in normal and TOF patients.

significant difference between regional shortening fractions in normal patients versus those with TOF (p < .00002) after allowing for effects of differences between regions. Eleven of the twelve regions showed decreased shortening in the TOF patients when compared to normals (p < .01). Upon subsequent paired analysis, these differences reached statistical significance in the mid- and apical-freewall regions (p < .05).

## 4. Discussion

The results of our study indicate that RV regional shortening is heterogeneous. In particular, the RV freewall contracts a great deal more than the septum, while the superior and inferior walls display intermediate levels of shortening (Fig. 1). This heterogeneity follows a consistent pattern from subject to subject, and normal regional shortening fractions can be established for each of the 12 standardized regions, with reasonable confidence intervals.

The contraction time, which we have indexed with t70, is also heterogeneous between regions, even in normal patients. While the LV tends to contract in a uniform fashion, our study has demonstrated that different portions of the normal RV contract at different times, even in the absence of a conduction delay, consistent with the study of Geva et al. (9) which demonstrated that the infundibulum contracts later than the body of the RV. Our inability to detect differences in average t70 between regions does not seem to support the notion that RV contraction time is homogeneous throughout the RV; rather, the lack of consistent region-to-region differences and the wide standard deviations of t70 within each region support the notion that RV contraction differs from person to person.

However, while the *time* to excitation-contraction coupling in a given region may be inconsistent from person to person, the region-to-region differences in *magnitude* of this contraction seem more consistent. Patients with TOF have a similar pattern of heterogeneity in their RV contraction, but the shortening is overall diminished compared to normal, on a region-to-region basis. Although we did not measure global
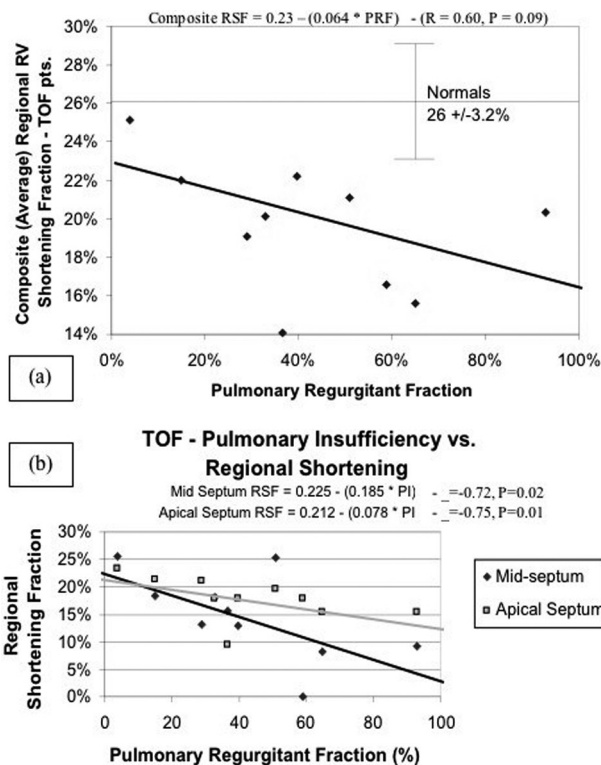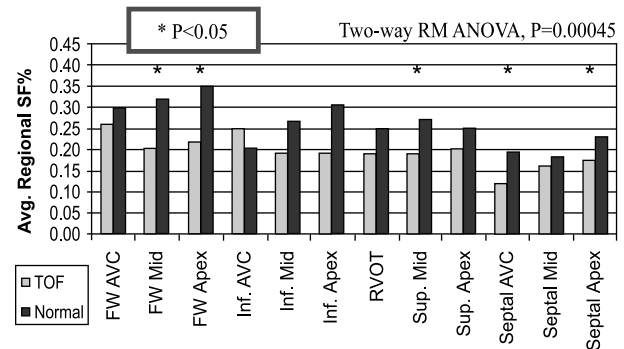
**Figure 5.** (a) The relationship of pulmonary insufficiency and composite (average) regional shortening fraction. The horizontal bar represents the average composite RSF of the normal patients as a reference. (b) Pulmonary insufficiency fraction in TOF patients correlates with regional shortening fractions in the mid- and apical-septum (ρ=.72 and .75, respectively).

ejection fractions or ventricular volumes, the degree of pulmonary insufficiency correlates to some degree with our composite RSF measurement. The patient with the least pulmonary insufficiency (PRF 4%) had the best composite RSF of the TOF patients. It is likely that the relationship between shortening and pulmonary insufficiency is best explained by the effect of ventricular volume on ejection fraction in patients with a given cardiac output. Larger ventricles need to contract to a smaller degree than smaller ventricles to produce a given stroke volume, a relationship which has been demonstrated in the past (26). However, this relationship cannot be applied to the volume overloaded RV in a simple manner because of the increased stroke volume of these ventricles.

Significant PI leads to increased preload and RV dilation, when compared with a similar RV without PI (given the same afterload, contractility, and heart rate), so global ejection fraction should be increased. The decreased systolic function in patients with TOF noted in previous studies, as well as the decreased composite RSF demonstrated in our TOF patients, suggest that the RV in TOF patients with PI is maladapted to this increased preload. These hearts may be working on a different Starling curve than the normal RV, with a greater end-systolic volume as well as a much greater end-diastolic volume. The inverse relationship between PI (which serves as an index of the volume loading condition of each heart) and composite RSF is consistent with this notion.

Septal RSF had a significant inverse correlation with PI, while other regions did not. It may be that because the septal wall is shared by both the RV and the LV, it is more affected by increased RV volume overload than other wall regions. Another factor may be sutures in the ventricular septal defect patch, which may have caused some damage to these regions.

Measuring RV function has always been problematic, and many techniques have been suggested. The technique described in our study, 1-D myocardial tagging, has a number of advantages over previously described techniques for measuring regional RV function, including its quantitative nature, the familiarity of the shortening fraction as a measurement, and the familiarity of the 4ch and RVLA views. Although our study maximized the accuracy of measurements by utilizing intensity mapping, routine use of this 1-D technique can be employed without such complicating factors. One can easily "eyeball" the centers of each stripe with reasonable accuracy and calculate shortening fractions quickly and easily.

It is often difficult to measure regional RV function using tools developed for measurement of regional LV function. For example, measuring regional wall motion in the LV utilizing grid-pattern spatial modulation of magnetization (SPAMM) relies on the thickness of the LV wall. Since the RV is normally a thin-walled structure, and two adjacent intersections will infrequently tag the normal RV wall, it is difficult to use grid tagging on the RV. As another example, echocardiography is frequently used to measure regional motion in the LV, but the difficulties in viewing the anterior wall of the RV underneath the sternum make this an ill-suited technique for measurement of even qualitative regional wall analysis. In addition, the LV has internal landmarks such as the papillary muscles which are more consistent than RV landmarks. Further, the complex shape of the RV makes assessment of regional motion by angiography quite difficult. It is therefore prudent to establish a set of unique tools suited for measurement of regional function specifically in the RV. The 1-D tagging technique described here provides insight into RV mechanics and may prove to be a useful clinical tool to the clinician.

In this study we used TOF patients with pulmonary insufficiency as a model of the volume loaded RV. TOF patients have decreased RSFs compared with normal patients on a region-by-region basis, consistent with studies of TOF from a global function standpoint. Regional function is important to understanding global function since regions which are hyperdynamic must make up for hypokinetic regions in order to leave global output unchanged. When comparing different groups of patients or different loading conditions, changes in global myocardial function (ejection fraction, stroke volume, etc.) may not be apparent despite significant changes in regional function.

These findings are consistent with previous studies of global right ventricular function in patients with TOF. In 1996, Niezen et al. (6) used MRI to study RV volumes in normals and TOF patients. They found a correlation between RV stroke volume and PI and also noted that patients with TOF had significantly larger end-diastolic and end-systolic RV volumes as well as reduced RV ejection fractions compared to normal patients, despite an increased stroke volume proportional to the degree of PI. These findings are consistent with our findings of reduced regional shortening and composite regional shortening fractions in TOF patients.

In our study, we found differences in regional systolic RV performance (e.g. base of the RV along the anterior and inferior freewall contracting greater than the septum). The contributions of the regions with greater RSFs are more important to total RV output than the ones with lower RSFs, and indeed, may compensate for these less contractile regions. One of this study's contributions is the ability to quantify such regional differences and describe the relative contributions of these various portions of the RV.

It will be interesting to compare our TOF patients to patients with other forms of RV volume overload, such as those with atrial septal defects or even even single RVs such as the shunted patient with hypoplastic left heart syndrome prior to cavopulmonary anastomosis.

## 4.1. *Limitations*

The relatively small number of patients, especially in the TOF group, limits our ability to separate results into age groups. Nevertheless, for pediatric patients as a group, our results

stand. Teasing out age-related differences will be a subject of further investigation.

The usefulness of TOF with PI as an example of the volume-loaded RV is limited because of the changes in the RV secondary to the ventriculotomy in the infundibulum and the ventricular septal defect patch. It will be interesting to study regional shortening in other RV volume-loading conditions such as atrial septal defect in order to determine the similarities of differences in regional RV performance between volume loading conditions. The authors appreciate that substantially dilated or pressure-loaded RVs may have unusual configurations. However, because our method measures motion in the base-to-apex direction, through-plane motion plays a very small role in both normal and dilated hearts.

TOF patients are a heterogeneous group in many ways. They have received different repairs at different ages, and their hemodynamics vary. We studied a diverse age group, and young patients may have less ventricular dysfunction after repair of TOF (29). We did not find a relationship between age and composite RSF. It was not possible to control for differences such as time of cardiopulmonary bypass, chronic cyanosis preceding repair, pressure loading prior to repair, or abnormal depolarization secondary to postoperative right bundle branch block (RBBB). Further study will be required to evaluate the relationship between age and regional ventricular dysfunction in TOF, and this 1-D tagging technique may be an ideal tool for such assessment.

MRI creates images of fixed planes in space and does not track through-plane motion during the cardiac cycle. Since our imaging planes were chosen to be parallel to the principal direction of myocardial travel, this through-plane motion plays a small role. In addition, the number of frames per cycle limits the temporal resolution when defining end-systole for calculations of RSF and t70. This limitation, again, plays a very small role in this study. However, it is important to note that myocardial motion is quite complex, and that this 1-D technique simplifies the assessment of myocardial shortening. We believe that the simplicity of our method of measurement, and the lack of specialized software requirements justify this simplification.

The reproducibility of our measurements remains to be determined. For our study, one observer made all measurements for all patients. Further study will be necessary to determine the amount of interobserver and intraobserver variability that can be expected using this technique, and how much variability may be expected from day to day within a given patient.

## 5. Conclusions

Normal regional RV systolic function is heterogeneous, with freewall portions of the RV contracting a greater amount than septal portions. MRI with 1-D myocardial tagging can be used to measure regional shortening fractions within the right ventricle. Normal regional shortening fractions can be established with reasonable confidence limits. Post-operative TOF patients, as a group, have decreased regional shortening fractions.

## References

1. D'Anfrea A, Ducceschi V, Caso P, Galderisi M, Mercurio B, Liccardo B, Sarubbi B, Scherillo M, Cotrufo M, Calabro R. Usefulness of tissue Doppler imaging for assessment of right and left ventricular myocardial function in patients with dual-chamber pacing. Int J Cardiol 2001; 81(1):75–83.
2. Mahle WT, Coon PD, Wernovsky G, Rychik J. Quantitative echocardiographic assessment of the performance of the functionally single right ventricle after the Fontan operation. Cardiol Young 2001; 11(4):399–406.
3. Abd El Rahman MY, Abdul-Khaliq H, Vogel M, Alexi-Meskischvili V, Gutberlet M, Hetzer R, Lange PE. Value of the new Doppler-derived myocardial performance index for the evaluation of right and left ventricular function following repair of tetralogy of Fallot. Pediatric Cardiology 2002; 23(5):502–507.
4. Kavey REW, Bove EL, Byrum CJ, Blackman MS, Sondheimer HM. Postoperative functional assessment of a modified surgical approach to repair of tetralogy of Fallot. J Thorac Cardiovasc Surg 1987; 93:533–538.
5. Denslow S, Wiles HB, McKellar LF, Wright NA, Gillette PC. Right ventricular volume estimation with an ellipsoidal shell model and two-plane magnetic resonance imaging. Am Heart J 1995; 129:782–790.
6. Niezen RA, Helbing HA, van der Wall EE, van der Geest RJ, Rebergen SA, de Roos A. Biventricular systolic function and mass studied with MR imaging in children with pulmonary regurgitation after repair of tetralogy of Fallot. Radiology 1996; 201:135–140.
7. Unterberg K, Plesak L, Voelker W, Karsch KR. Quantitative segmental analysis of wall function of the right ventricle in probands with healthy hearts. [German]. Z Kardiol 1988; 77(2):120–124.
8. Karwatowski SP, Mohiaddin R, Yang GZ, Firmin DN, Sutton MS, Underwood SR, Longmore DB. Assessment of regional left ventricular long axis motion with MR velocity mapping in healthy subjects. JMRI 1994; 4:151–155.
9. Geva T, Powell AJ, Crawford EC, Chung T, Colan SD. Evaluation of regional differences in right ventricular systolic function by acoustic quantification echocardiography and cine magnetic resonance imaging. Circulation 1998; 98(4):339–345.
10. Fogel MA, Gupta KB, Weinberg PM, Hoffman EA. Regional wall motion and strain analysis across stages of Fontan reconstruction by magnetic resonance tagging. Am J Physiol 1995; 269:H1132–H1152.
11. Fogel MA, Weinberg PM, Fellows KE, Hoffman EA. A study in ventricular–ventricular interaction: single right ventricles compared with systemic right ventricles in a dual-chamber circulation. Circulation 1995; 92:219–230.
12. Kukulski T, Hubert L, Arnold M, Wranne B, Hatle L, Sutherland GR. Normal regional right ventricular function and its change with age: a Doppler myocardial imaging study. J Am Soc Echocardiogr 2000; 13(3):194–204.
13. Vignon P, Weinert L, Mor-Avi V, Spencer KT, Bednarz J, Lang RM. Quntitative assessment of regional right ventricular function with color kinesis. Am J Respir Crit Care Med 1999; 159(6):1949–1959.
14. Weidemann F, Eyskens B, Mertens L, Dommke C, Kowalski M, Simmons L, Claus P, Bijnens B, Gewillig M, Hatle L, Sutherland GR. Quantification of regional right and left ventricular function by ultrasonic strain rate and strain indexes after surgical repair of tetralogy of Fallot. Am J Cardiol 2002; 90(2):133–138.
15. Fischer SE, McKinnon GC, Scheidegger MB, Prins W, Meier D, Boesiger P. True myocardial motion tracking. Magn Reson Med 1994; 31:401–413.

16. Bogaert J, Bosmans H, Maes A, Suetens P, Marchal G, Rademakers FE. Remote myocardial dysfunction after acute anterior myocardial infarction: impact of left ventricular shape on regional function. J Am Coll Cardiol 2000; 35(6):1525–1534.

17. Verhnet H, Revel D, Arteaga C, et al. Predictive value of left ventricular circumfrential shortening in jeopardized myocardium—a two-dimensional SPAMM cine-MRI study in a canine model. Invest Radiol 1999; 34(10):621–628.

18. Zerhouni EA, Parish DM, Rogers WJ, Yang A, Shapiro EP. Human heart: tagging with MR imaging: a method for noninvasive assessment of myocardial motion. Radiology 1988; 169:59–63.

19. Osman NF, Sampath S, Atalar E, Prince JL. Imaging longitudinal cardiac strain on short-axis images using strain-encoded MRI. Magn Reson Med 2001; 46:324–334.

20. Fogel MA, Weinberg PM, Hubbard A, Haselgrove J. Diastolic biomechanics in normal infants utilizing MRI tissue tagging. Circulation 2000; 102:218–224.

21. Axel L, Doughery L. MR imaging of motion with spatial modulation of magnetization. Radiology 1989; 171:841–845.

22. Lange PE, Onnasch DGW, Bernhard A, Heintzen PH. Left and right ventricular adaption to right ventricular overload before and after surgical repair of tetralogy of Fallot. Am J Cardiol 1982; 50:786–794.

23. Helbing WA, Niezen RA, LeCessie S, van der Geest RJ, Ottenkamp J, de Roos A. Right ventricular diastolic function in children with pulmonary regurgitation after repair of tetralogy of Fallot: volumetric evaluation by magnetic resonance velocity mapping. JACC 1996; 28(7):1827–1835.

24. Eyskens B, Reybrouck T, Bogaert J, Dymarkowsky S, Daenen W, Dumoulin M, Gewillig M. Homograft insertion for pulmonary regurgitation after repair of tetralogy of Fallot improves cardiorespiratory performance. Am J Cardiol 2000; 85: 221–225.

25. Wessel HU, Paul MH. Exercise studies in tetralogy of Fallot: a review. Pediatr Cardiol 1999; 20:39–47.

26. Schamberger MS, Hurwitz RA. Course of right and left ventricular function in patients with pulmonary insufficiency after repair of tetralogy of Fallot. Pediatr Cardiol 2000; 21:244–248.

27. Bove EL, Byrum CJ, Thomas FD, Kavey RE, Sondheimer HM, Blackman MS, Parker FB Jr. The influence of pulmonary insufficiency on ventricular function following repair of tetralogy of Fallot—evaluation using radionuclide ventriculography. J Thorac Cardiovasc Surg 1983; 85:691–696.

28. Rebergen SA, Chin JGJ, Ottenkamp J, van der Wall EE, de Roos A. Pulmonary regurgitation in the late postoperative follow-up of tetralogy of Fallot—volumetric quantification by nuclear magnetic resonance velocity mapping. Circulation 1993; 88(pt 1):2257–2266.

29. Sarubbi B, Pacileo G, Pisacane C, Ducceschi V, Iacono C, Russo MG, Iacono A, Calabrò R. Exercise capacity in young patients after total repair of tetralogy of Fallot. Pediatr Cardiol 2000; 21:211.

30. Hoffman EA, Gnanaprakasam D, Gupta KB, et al. VIDA. An environment for multidimensional image display and analysis. Proc SPIE 1992; 1660:694–711.